arXiv:1412.8289v1 [cond-mat.mes-hall] 29 Dec 2014

Domain wall magneto-Seebeck effect

Patryk Krzysteczko,* Xiukun Hu, Niklas Liebing, Sibylle Sievers, and Hans W. Schumacher
Physikalisch-Technische Bundesanstalt, Bundesallee 100, D-38116 Braunschweig, Germany

The interplay between charge, spin, and heat currents in magnetic nano systems subjected to a temperature gradient has lead to a variety of novel effects and promising applications studied in the fast-growing field of spincaloritronics. Here we explore the magnetothermoelectrical properties of an individual magnetic domain wall in a permalloy nanowire. In thermal gradients of the order of few K/µm along the long wire axis, we find a clear magneto-Seebeck signature due to the presence of a single domain wall. The observed domain wall magneto-Seebeck effect can be explained by the magnetization-dependent Seebeck coefficient of permalloy in combination with the local spin configuration of the domain wall.

Electronic transport coefficients in ferromagnetic materials are spin-dependent[1] enabling important spintronics applications[2]. This observation also holds for magnetothermoelectric (or spincaloritronic) phenomena[3–5], driven by thermal gradients[6–9]. In a thermal gradient, the temperature difference ΔT between two contacts gives rise to a thermopower $V_{\mathrm{T}} = -S\Delta T$ with S being the material's Seebeck coefficient. Spin-dependent Seebeck coefficients have been observed in various nanomagnetic systems like thin films[10,11], multilayers[12], tunnel junctions[13–15], and nanowires[16,17]. In the latter, magnetization reversal often occurs by the nucleation and propagation of a single magnetic domain wall (DW) enabling promising applications[18–20]. Also a DW can interact with a thermal gradient[21–23] with prospects for thermally driven DW motion[24–27] or nanoscale magnetic heat engines[28]. However, the fundamental thermoelectrical properties of an individual magnetic DW have not been investigated yet.

In our experiments we use L-shaped permalloy (Py) nanowires with a notch (see Fig. 1A and supplementary material for details). The L's corner allows a controlled nucleation of a DW while the notch allows pinning a moving DW between the electrical probes. The two probes are contacting the Py wire from the top for resistance and thermopower measurements. Two additional Pt strips located at a distance of 0.5 µm and 1.5 µm from the Py nanowire serve as resistive thermometer and heater, respectively. The magnetic behavior of the system is characterized by two-wire resistance measurements as a function of magnetic field at a DC current of 600 µA. In a first step, the magnetization of the entire wire is rotated from the longitudinal ($\parallel$) to the transversal ($\perp$) direction by a magnetic field applied at $\phi = 90°$, i.e. along the y-direction (note the definition of coordinates in Fig. 1A). As expected for a system dominated by the anisotropic magnetoresistance (AMR), the measurement shows a bell-shaped curve (Fig. 2A) with resistance being decreased by the field of either polarity by $\Delta R = R_{\parallel} - R_{\perp}$. We find $R_{\parallel} = 289.8\,\Omega$ at remanence and $R_{\perp} = 288.5\,\Omega$ at maximum transversal field and hence a two-wire AMR ratio $\Delta R/R_{\perp} = 0.45\,\%$. In a second step, we study the AMR contribution of a single DW. For this purpose we apply a 120 mT field in diagonal direction ($\phi_{\mathrm{set}} = -135°$) to create a head-to-head DW at the corner which is than moved towards the notch by a field applied at any $|\phi| < 80°$. As an example, Fig. 2B shows a measurement at $\phi = 0°$. The DW arrives at the notch at H_1, where it remains until H_2 is reached. The presence of the DW at the notch leads to a decrease of resistance by approximately $0.17\,\Omega$. The resistance drop is due to transversally oriented magnetization within the DW and based entirely on AMR. The critical fields H_1 and H_2 are the pinning fields of the corner and of the notch, respectively. To fully characterize the DW dynamics we repeat the measurement in the angle-range $|\phi| < 80°$. The results are presented in Fig. 1C, where the resistance is indicated by a color-scale. The yellow region indicates the resistance lowered due to the presence of the DW at the notch. Typically the left edge of this region is smooth whereas the right edge is rather irregular. This means that the pinning strength of the corner $H_1(\phi)$ for various angles is well defined[29] whereas the pinning strength of the notch $H_2(\phi)$ has a stronger stochastic component. We model the magnetization distribution during field-driven DW motion by micromagnetic simulations using a Landau-Lifshitz-Gilbert micromagnetic simulator[30]. Our numerical analysis predicts that a vortex-type of DW is nucleated at the corner as pictured in Fig. 3D, where a snapshot of the magnetization distribution at $\mu_0 H = 20\,\mathrm{mT}$ during a field sweep at $\phi = -30°$ is shown. For increasing field strength, the vortex DW will be 'pulled' deeper into the notch, deformed and finally transformed into a transversal DW before depinning, which explains the stochastic behavior of $H_2(\phi)$.

For thermoelectrical measurements, we generate temperature gradients by applying an AC power P at a frequency of $f = 262\,\mathrm{Hz}$ to the heater. To characterize the temperature distribution we use calibration samples with identical heaters and thermometers placed correspondingly to the positions of the voltage probes (red lines in Fig. 1A). For each heater power P, the thermometer resistance has a $2f$ AC component with amplitude $\delta R(P)$ detected by 4-wire lock-in measurements. To translate δR to the temperature increase δT we first determine the temperature coefficient α_{Pt} in a separate setup. We find $\alpha_{\mathrm{Pt}} = 0.0013\,\mathrm{K}^{-1}$ which is 30 % of the bulk value in good agreement with literature[31]. Figure 1B shows the measured δT (blue bullets) as a function of the distance d from the heater for three heating powers: 17 mW, 22 mW and 27 mW. The temperature distribution is further investigated by three-dimensional finite-

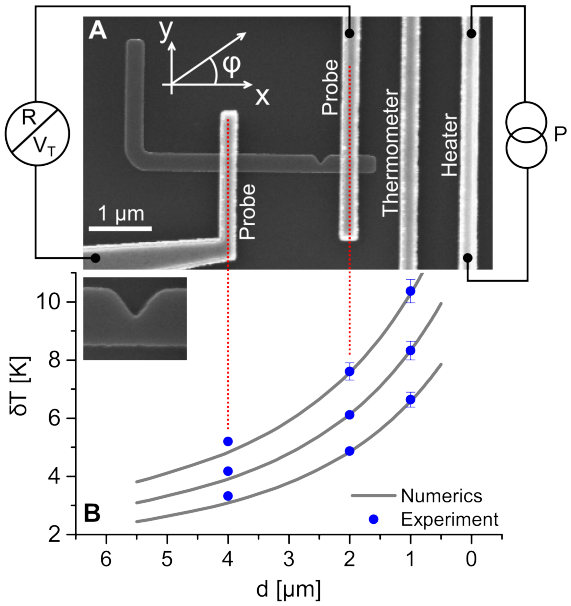

FIG. 1: Sample geometry and temperature distribution. (A) Micrograph of the L-shaped permalloy nanostructure with Pt contact probes for voltage and resistance measurement. The inset below shows the notch with higher magnification. (B) The temperature increase for three heater powers $P = 17$, 22, and 27mW as a function of the distance to the heater. Experimental results are shown by blue bullets; numerical results (grey lines) show a good agreement.

element modeling. The numerical results (gray lines) show a good agreement with the experimental data. Heating with 27 mW accordingly leads to an increase of the nanowire temperature of up to 10 K and a ΔT between the probes of (2.4 ± 0.5) K. In the following, the thermopower V_T is measured at $P = 27$ mW by lock-in detection at $2f$ via the voltage probes.

Figure 2D shows the evolution of the thermopower V_T as a function of transversal field ($\phi = 90°$, cf. Fig. 2A). Again, a bell-shaped curve comes into view, but with the thermopower being *increased* by a magnetic field of either polarity. We find a thermopower of $V_{\mathrm{T}\parallel} = 56.08\,\mu\mathrm{V}$ at remanence and $V_{\mathrm{T}\perp} = 56.54\,\mu\mathrm{V}$ at maximum field with an accuracy of ± 10 nV. The effective Seebeck coefficient is $S = (23 \pm 6)\,\mu\mathrm{V/K}$. The magnetothermopower (MTP) ratio $(V_{\mathrm{T}\parallel} - V_{\mathrm{T}\perp})/V_{\mathrm{T}\perp}$ yields $(-0.81 \pm 0.03)\,\%$. The Seebeck coefficient of the nanowire thus rises when the wire's magnetization rotates under the action of an external field. For comparison of magnetoresistance (MR) and magento-Seebeck ratio the lead contributions have to be taken into account as discussed in the supplementary material. In the following we investigate the change of thermopower induced by the presence of a single DW. As an example, Fig. 2E shows a MTP measurement at the same conditions as the MR measurement shown in Fig. 2B. As the field reaches $\mu_0 H = 4$ mT, we observe a sudden increase of thermopower by approx. 40 nV. The thermopower remains roughly constant at this level until the field reaches 21 mT, where it drops back to the base level. Figure 2F shows the complete set of DW thermopower (DWTP) measurements for angles $|\phi| < 80°$. In this color plot, the yellow area indicates the increased thermopower. If we compare the pinning fields from MR and thermopower measurements (Figs. 2C and 2F), and keep the stochastic nature of H_2 in mind, we can safely consider them as identical. Evidently the origin of increased thermopower is the same as the origin of reduced resistance, namely the presence of a DW at the notch. The data thus clearly reveal the thermoelectrical signature of a single DW.

To analyze our data, we describe the thermopower of a system magnetized along the x-direction by

$$\nabla V_\mathrm{T} = -\begin{pmatrix} S_\parallel & & \\ & S_\perp & -S_N \\ & S_N & S_\perp \end{pmatrix} \nabla T\,, \tag{1}$$

where the Seebeck coefficient has tensor character analogous to the resistivity tensor (see supplementary material). The diagonal elements of the tensor represent the anisotropy of the Seebeck coefficient; $S_\parallel$ is measured when the temperature gradient is parallel to the magnetization direction while $S_\perp$ is measured when it is transversal to the magnetization direction (cf. Fig. 2d). We consider also the anomalous Nernst effect (ANE) by the off-diagonal

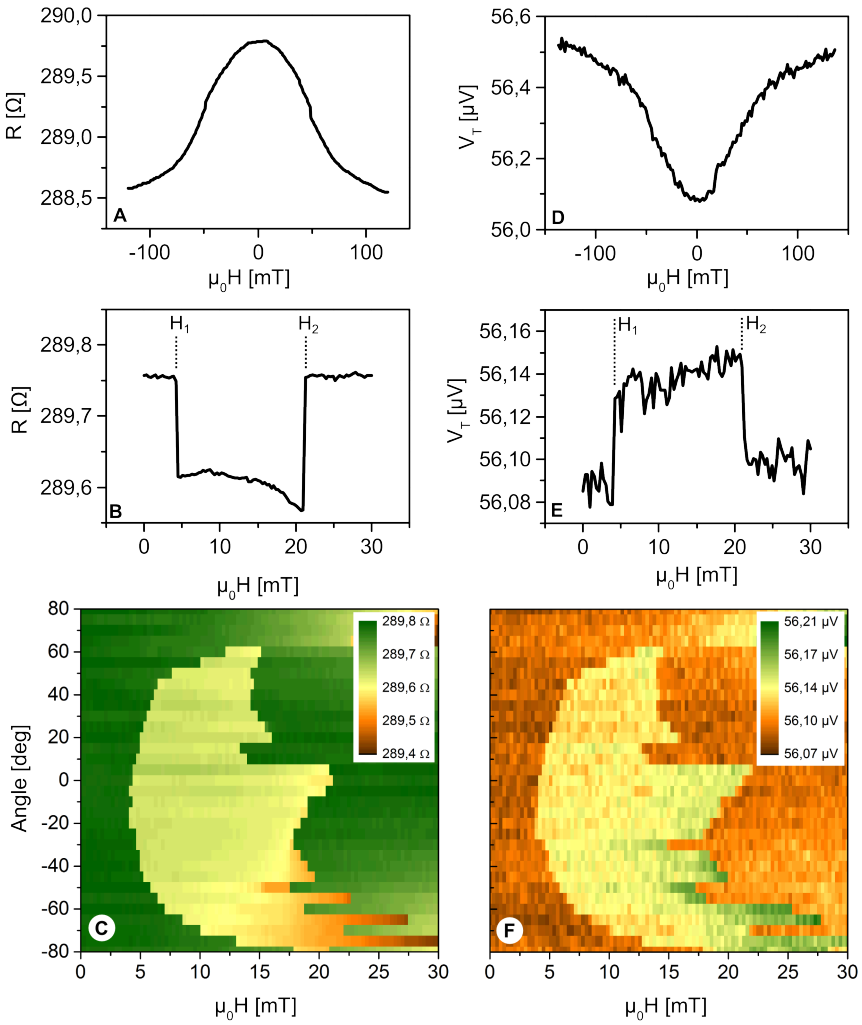

FIG. 2: Magnetoresistance and magnetothermopower measurement. (A) The resistance R of the wire vs. applied field $\mu_0 H$ measured in transversal geometry ($\phi = 90°$) (B) Domain wall magnetoresistance measured at $\phi = 0°$. The pinning fields of the corner and the notch are indicated by H_1 and H_2, respectively. (C) A set of domain wall magnetoresistance measurements for angles $|\phi| < 80°$. The resistance is indicated by the color scale. (D) The thermopower of the wire measured in transversal geometry ($\phi = 90°$) (E) Domain wall magnetoresistance measured at $\phi = 0°$. (F) A set of domain wall magnetothermopower measurements for all angles $|\phi| < 80°$. The thermopower is indicated by the color scale.

elements $S_N = -2.6\,\mu\mathrm{V/K}$, which will generate an additional thermopower in the case of a non-vanishing out-of-plane temperature gradient[32]. Our experimental setup is designed to detect the thermopower generated along the wire direction thus we consider only the x-component of Eq. 3. The resulting MTP can be described by three terms

$$\begin{aligned} V_\mathrm{T} \;=\; & -\left(S_\perp + \Delta S \cos^2(\theta)\right) \Delta T_x \\ & -\Delta S \cos(\theta)\sin(\theta)\,\Delta T_y \\ & -S_N \sin(\theta)\,\Delta T_z\,, \end{aligned} \tag{2}$$

where θ is the angle of the local magnetization direction with respect to the x-direction (see supplementary material). Due to the analogy with AMR, we refer to the first term as anisotropic magneto-Seebeck (AMS) effect. The second term is related to the planar Nernst effect (PNE)[10] and the third term describes the ANE contribution of an in-plane magnetized system. We use our numerical results of magnetization distribution and temperature gradients to verify this approach. The nanowire is divided in cells of $10 \times 10\,\mathrm{nm}^2$. For each cell we take the local magnetization direction $\theta(x, y)$ and the temperature difference across the cell to calculate the local thermopower according to Eq. 2. To estimate the global thermopower, we calculate the mean thermopower generated in each 10-nm-slice of the wire and sum over all slices between the voltage probes. We repeat those calculations for various magnetic configurations (cf.

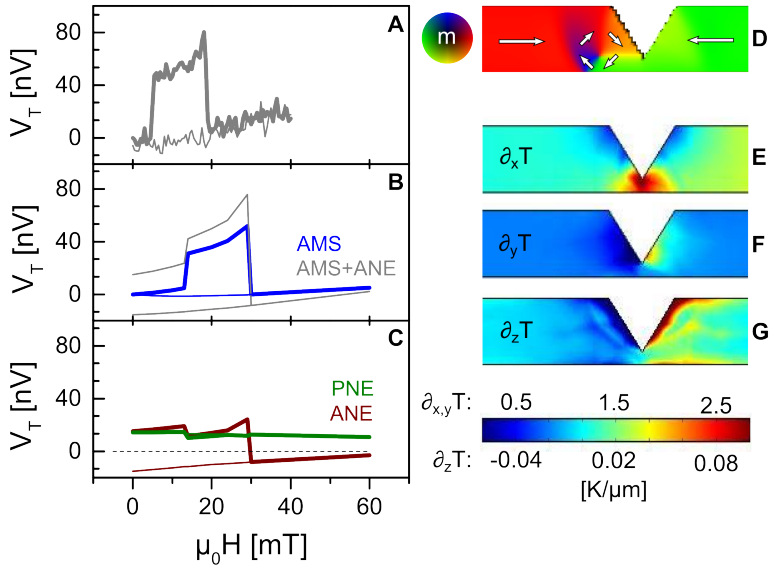

FIG. 3: (A) Domain wall magnetothermopower measured at $\phi = -30°$. The graph shows the thermopower change with respect to the remanent state $V_{T\parallel}$. (B) The calculated AMS contribution (blue) and the calculated contribution due to AMS and ANE acting together (grey). (C) Calculated contribution due to PNE (green) and ANE (brown). (D) Example of a simulated magnetization distribution showing a vortex DW. The local magnetization direction is indicated by the color scale. (E-G) The calculated temperature gradient in x, y and z-direction.

Fig. 3D) corresponding to the movement of a DW during a field-sweep at $\phi = -30°$. The temperature gradients are shown as a color map in Fig. 3E–G (note the different color scales for in-plane and out-of-plane directions).

Figure 3A shows the measured DWTP for $\phi = -30°$ with the thermopower of the remanent state $V_{T\parallel}$ set to zero. The calculation considering only the AMS is shown in Fig. 3B by the blue curve. Considering the typical deviations of a micromagnetic model a very good agreement between experiment and simulation is obtained. Our analysis thus reveals that the DWTP is dominated by the AMS (first term in Eq. 2) and the remaining terms of Eq. 2 are treated as corrections. The expected PNE contribution is indicated by the green line in Fig. 3C. It shows a nearly constant value of approx. 15 nV with a DW signature of only 3 nV. Within the experimental noise level, PNE should hence have no impact on the DWTP. Figure 3C also plots the ANE contribution (brown line). At $\mu_0 H = 0$ mT the ANE has a value of about 15 nV. During the DW pinning only a small change of the ANE signal occurs. However, at 30 mT the ANE signal shows a sudden drop and a change of sign. Here the magnetization direction at the hot side of the notch is reversed due to the depinning of the DW. In the following up-sweep to 60 mT and the back-sweep to 0 mT a linear behavior is found. ANE should thus lead to a splitting of the signal at zero field. Taking into account both, AMS and ANE, leads to the grey curve in Fig. 3B. Clearly, this splitting predicted at low fields is not observed in the experiment. From that we can conclude that the ANE is not significant in the experimental data and seems to be overestimated by the model. Note that the temperature model is based on a wire with sharp rectangular cross sections and a sharp V-shaped notch. This leads to an overestimation of the out-of-plane gradients at the notch and hence of the ANE contribution compared to the real device with rounded edges and smooth notch (cf. Fig. 1B, inset).

Similar results have been obtained on various devices with varying geometries confirming that a slight variation of the nanowire width or the notch shape does not change the general behavior. Furthermore, no significant difference between head-to head and tail-to-tail DWs was found. Our data thus clearly reveal the thermopower contribution of an individual DW in a magnetic nanowire thereby providing the fundamental link between macroscopic thermoelectrical signature and nanomagnetic spin configuration.

* Electronic address: patryk.krzysteczko@ptb.de

[1] N. F. Mott and H. Jones, *Theory of the properties of metal and alloys* (Oxford University Press, 1953).
[2] I. Zutic, J. Fabian, and S. D. Sarma, Rev. Mod. Phys. **76** (2004).
[3] M. Johnson and R. H. Silsbee, Phys. Rev. B **35**, 4959 (1987).
[4] G. E. W. Bauer, A. H. MacDonald, and S. Maekawa, Solid State Commun. **150**, 459 (2010).
[5] G. E. W. Bauer, E. Saitoh, and B. J. van Wees, Nature Materials **11**, 391 (2012).

[6] K. Uchida, Nature **455**, 778 (2008).
[7] A. Slachter, F. L. Bakker, J. P. Adam, and B. J. van Wees, Nature Phys. **6**, 879 (2010).
[8] J.-C. LeBreton, S. Sharma, H. Saito, S. Yuasa, and R. Jansen, Nature **475**, 82 (2011).
[9] K.-R. Jeon, B.-C. Min, A. Spiesser, H. Saito, S.-C. Shin, S. Yuasa, and R. Jansen, Nature Materials **13**, 360 (2014).
[10] A. D. Avery, M. R. Pufall, and B. L. Zink, Phys. Rev. Lett. **109**, 196602 (2012).
[11] M. Schmid, S. Srichandan, D. Meier, T. Kuschel, J.-M. Schmalhorst, M. Vogel, G. Reiss, C. Strunk, and C. H. Back, Phys. Rev. Lett. **111**, 187201 (2013).
[12] J. Shi, R. C. Yu, S. S. P. Parkin, and M. B. Salamon, J. Appl. Phys. **73**, 5524 (1993).
[13] M. Czerner, M. Bachmann, and C. Heiliger, Phys. Rev. B **83**, 132405 (2011).
[14] M. Walter, J. Walowski, V. Zbarsky, M. Muenzenberg, M. Schaefers, D. Ebke, G. Reiss, A. Thomas, P. Peretzki, M. Seibt, et al., Nature Materials **10**, 742 (2011).
[15] N. Liebing, S. Serrano-Guisan, K. Rott, G. Reiss, J. Langer, B. Ocker, and H. W. Schumacher, Phys. Rev. Lett. **107**, 177201 (2011).
[16] T. Böhnert, V. Vega, A.-K. Michel, V. M. Prida, and K. Nielsch, Appl. Phys. Lett. **103**, 092407 (2013).
[17] L. Gravier, S. Serrano-Guisan, F. Reuse, and J. P. Ansermet, Phys. Rev. B **73**, 024419 (2006).
[18] T. Ono, H. Miyajima, K. Shigeto, K. Mibu, N. Hosoito, and T. Shinjo, Science **284**, 486 (1999).
[19] D. A. Allwood, G. Xiong, C. C. Faulkner, D. Atkinson, D. Petit, and R. P. Cowburn, Science **309**, 1688 (2005).
[20] S. S. P. Parkin, M. Hayashi, and L. Thomas, Science **320**, 190 (2008).
[21] L. Berger, J. Appl. Phys. **58**, 450 (1985).
[22] M. Hatami, G. E. W. Bauer, Q. Zhang, and P. J. Kelly, Phys. Rev. Lett. **99**, 066603 (2007).
[23] A. Kovalev and Y. Tserkovnyak, Phys. Rev. B **80**, 100408R (2009).
[24] D. Hinzke and U. Nowak, Phys. Rev. Lett. **107**, 027205 (2011).
[25] P. Yan, X. S. Wang, and X. R. Wang, Phys. Rev. Lett. **107**, 177207 (2011).
[26] J. Torrejon, G. Malinowski, M. Pelloux, R. Weil, A. Thiaville, J. Curiale, D. Lacour, F. Montaigne, and M. Hehn, Phys. Rev. Lett. **110**, 177202 (2013).
[27] W. Jiang, P. Upadhyaya, Y. Fan, J. Zhao, M. Wang, L.-T. Chang, M. Lang, K. L. Wong, M. Lewis, Y.-T. Lin, et al., Phys. Rev. Lett. **110**, 177202 (2013).
[28] G. E. W. Bauer, S. Bretzel, A. Brataas, and Y. Tserkovnyak, Phys. Rev. B **81**, 024427 (2010).
[29] H. Corte-Leon, V. Nabaei, A. Manzin, J. Fletcher, P. Krzysteczko, H. W. Schumacher, and O. Kazakova, Sci. Rep. **4**, 6045 (2014).
[30] M. R. Scheinfein, J. Unguris, J. L. Blue, K. J. Coakley, D. Pierce, R. J. Celotta, and P. Ryan, Phys. Rev. B **43**, 3395 (1991).
[31] X. Zhang, H. Xie, M. Fujii, H. Ago, K. Takahashi, T. Ikuta, H. Abe, and T. Shimizu, Appl. Phys. Lett. **86**, 171912 (2005).
[32] A. Slachter, F. L. Bakker, and B. J. van Wees, Phys. Rev. B **84**, 020412 (2011).
[33] A. Soni and G. S. Okram, Rev. Sci. Inst **79**, 125103 (2008).
[34] C. Y. Ho, M. W. Ackerman, K. Y. Wu, S. G. Oh, and T. N. Havill, J. Phys. Chem. Ref. Data **7**, 959 (1978).
[35] E. A. Owen, E. L. Yates, and A. H. Sully, Proc. Phys. Soc. **49**, 315 (1937).
[36] D. Bonnenberg, K. A. Hempel, and H. P. J. Wijn, *Springer Materials: The Landolt-Brönstein Database* (Springer, 2000).
[37] S. Hankenmeier, K. Sachse, Y. Stark, R. Frömter, and H. Oepen, Appl. Phys. Lett. **92**, 242503 (2008).
[38] J. Banhart and H. Ebert, Europhys. Lett. **32**, 517 (1995).

Supplementary material

A. Device Fabrication

In our experiments we use an L-shaped Py nanowire with a notch. The nanowire is 290 nm wide and has arms of 2 µm and 4 µm length. The longer arm has a notch, 150 nm deep and 280 nm wide, at a distance of 3 µm from the corner. The nanostructure is patterned by electron beam lithography in combination with Ar ion etching from a continuous Py film that has been sputter-deposited on a 525 µm Si substrate covered by a 50 nm SiO layer. The Py is 27 nm thick and covered with a Pt cap of 2 nm to prevent oxidation. Additionally, devices without Pt cap were fabricated to ensure that the Pt capping layer has no significant influence on the DWTP. In a second lithography step, we attach Pt wires as voltage probes. The Pt wires are 115 nm thick with a 10 nm Ta adhesion layer. The interface between Py and Ta is cleaned in-situ by low energy Ar ions prior to Ta/Pt deposition to ensure good electrical contact. Two additional Pt strips located at a distance of 0.5 µm and 1.5 µm from the Py nanowire serve as resistive thermometer and heater, respectively.

B. Temperature calibration

To detect the temperature gradient experimentally, at least two thermometers are needed, each sensitive to the temperature T_d at a certain distance d from the heat source. We fabricate a set of nominally identical devices with heater-thermometer pairs separated by 1 µm, 2 µm and 4 µm. For each distance, the calibration is repeated for four different devices to increase the statistical significance. The temperature coefficient of the Pt thermometer α_{Pt} is measured by 4-wire resistance R measurements as a function of the temperature T of a hot plate heated to up to 30 K above room temperature. We use thermal grease and an equilibration time of at least 30 min to ensure uniform temperature distribution before taking a $R(T)$ value. The resulting temperature coefficient $0.00125\,\mathrm{K}^{-1} < \alpha_{\mathrm{Pt}} < 0.00135\,\mathrm{K}^{-1}$ allows for a measurement of the local temperature increase δT with an accuracy of approx. ±4 %. This results in an uncertainty of the temperature difference ΔT measured between $d = 4\,\mu\mathrm{m}$ and $d = 2\,\mu\mathrm{m}$ of approx. ±20 %. This uncertainty is not to be confused with poor time-stability.

C. The influence of the wiring

The 2-wire AMR ratio $(R_\parallel - R_\perp)/R_\perp$ is 0.45 %. This value, however, is obscured by the resistance of the wiring which is estimated on the basis of 4-wire measurements on similar devices to $R_{\mathrm{wire}} = 195.6\,\Omega$. This yields a 4-wire AMR ratio of 1.4 %.

Also the measured Seebeck coefficients are influenced by the electrical contacts. Considering a temperature gradient with $\Delta T = 2.4\,\mathrm{K}$, the nominal Seebeck coefficient of the permalloy-platinum thermocouple is $S_\parallel = -V_\parallel/\Delta T = -23.4\,\mu\mathrm{V/K}$ and $S_\perp = -V_\perp/\Delta T = -23.6\,\mu\mathrm{V/K}$ for the longitudinal and transversal geometry, respectively. This yields a magneto-Seebeck ratio $(S_\parallel - S_\perp)/S_\perp$ of −0.8 %. The Pt voltage probe contributes its own thermopower of 10.8 µV due to a Seebeck coefficient of $S_{\mathrm{Pt}} = -4.5\,\mu\mathrm{V/K}$[33]. The resulting absolute Seebeck coefficients of permalloy are $S_\parallel^{\mathrm{Py}} = -18.9\,\mu\mathrm{V/K}$ and $S_\perp^{\mathrm{Py}} = -19.1\,\mu\mathrm{V/K}$ with an uncertainty of ±5 µV/K. This yields an absolute magneto-Seebeck ratio of (-1.0 ± 0.05) %.

D. Modeling

For micromagnetic simulations we use a commercial micromagnetic modeling tool (LLG Micromagnetics Simulator)[30] with the following parameters: saturation magnetization $\mu_0 M_S = 1.005\,\mathrm{T}$, exchange stiffness $A = 1.05 \times 10^{-11}\,\mathrm{J/m}$, and uniaxial anisotropy constant $K_u = 100\,\mathrm{J/m^3}$ oriented along the long wire. The cells size is $10 \times 10 \times 25\,\mathrm{nm^3}$. The simulation temperature is zero Kelvin.

The temperature distribution is modeled by a commercial finite-element modeling tool (COMSOL Multiphysics). The input parameters are displayed in Tab. I. The boundary condition 'convective cooling' is activated for all surfaces in contact with air. The temperature of the air and of the bottom surface of the SiO substrate is fixed at 300 K.

Parameter	Permalloy	SiO	Si
Thermal conductivity [W/K m]	46.4[34]	1.4	130
Density [kg/m^3]	8700[35]	2200	2329
Heat capacity [J/kg K]	430[36]	730	700
Electrical conductivity [S/m]	4×10^6[37]	0	4×10^{-12}

TABLE I: Material parameters used for calculation of temperature distribution. Values for Si and SiO are taken directly from the COMSOL software. For Py we use literature values, as indicated.

E. The Seebeck tensor

An n-type conductor placed in a temperature gradient ∇T generally accumulates negative charge at the cool side leading to an electrical field $\vec{E}$ pointing away from the heat source. The efficiency of this process is described by the Seebeck coefficient S with $\vec{E} = S\,\nabla T$ (by this definition the Seebeck coefficient is negative for n-type conductors). It is customary to use $\vec{E} = -\nabla T_\mathrm{T}$ and rewrite this equation to $\nabla V_\mathrm{T} = -S\,\nabla T$ which by integration directly leads to the measured voltage $V_\mathrm{T} = -S\,\Delta T$. This voltage, which is referred to as thermopower, is generated between two points with a temperature difference of ΔT.

Our phenomenological description of the magneto-Seebeck effect is based on the according description of the magnetoresistance[38]. The Seebeck tensor for systems with the magnetization along the x-direction has the form

$$\nabla V_\mathrm{T} = -\begin{pmatrix} S_\parallel & & \\ & S_\perp & -S_N \\ & S_N & S_\perp \end{pmatrix} \nabla T \tag{3}$$

where S_N is a measure of the anomalous Nernst effect. $S_\parallel$ and $S_\perp$ are the longitudinal and transversal Seebeck coefficients, respectively. For a magnetization vector pointing in an arbitrary direction in the xy-plane we need to transform the Seebeck tensor S using the rotational matrix D_θ with θ the angle of the magnetization in respect to the x-axis

$$\nabla V_\mathrm{T} = -\mathsf{D}_\theta \mathsf{S} \mathsf{D}_\theta^{-1}\,\nabla T\,. \tag{4}$$

Using $\Delta S = S_\parallel - S_\perp$ this result can be written as

$$\nabla V_\mathrm{T} = -\begin{pmatrix} S_\perp + \Delta S\cos^2(\theta) \\ \Delta S\cos(\theta)\sin(\theta) \\ -S_N\sin(\theta) \end{pmatrix} \partial_x T - \begin{pmatrix} \Delta S\cos(\theta)\sin(\theta) \\ S_\perp + \Delta S\sin^2(\theta) \\ S_N\cos(\theta) \end{pmatrix} \partial_y T - \begin{pmatrix} S_N\sin(\theta) \\ -S_N\cos(\theta) \\ S_\perp \end{pmatrix} \partial_z T\,. \tag{5}$$

In our devices we are sensitive to the x-component of this vector which yields

$$V_\mathrm{T} = -\left(S_\perp + \Delta S\cos^2(\theta)\right)\Delta T_x - \Delta S\cos(\theta)\sin(\theta)\,\Delta T_y - S_N\sin(\theta)\,\Delta T_z\,. \tag{6}$$

We use the experimental results $S_\perp = -23.6\,\mu\mathrm{V/K}$ and $\Delta S = 0.2\,\mu\mathrm{V/K}$ as well as $S_N = -2.6\,\mu\mathrm{V/K}$ taken from literature[32].